Refractive-index nonlinearities of intersubband transitions in GaN/AlN quantum-well waveguides

Yan Li, Anirban Bhattacharyya, Christos Thomidis, Yitao Liao, Theodore D. Moustakas, and Roberto Paiella[a)]

Department of Electrical and Computer Engineering and Photonics Center, Boston University, 8 St. Mary's Street, Boston, Massachusetts 02215, USA

(Received 24 June 2008; accepted 19 August 2008; published online 16 October 2008)

The refractive-index nonlinearities of intersubband transitions in GaN/AlN quantum-well waveguides are investigated. A large spectral broadening of TM-polarized near-infrared pulses is observed after propagation through these devices due to intersubband self-phase modulation. From the measured data, a nonlinear refractive index n_2 of 1.8×10^{-12} cm^2/W is estimated at the operating wavelength of 1550 nm. A detailed theoretical model of the intersubband refractive index as a function of wavelength and optical intensity is then presented. This model assumes an inhomogeneously broadened transition line and is based on experimentally determined material and device parameters. The results of this study are finally used to discuss the prospects of nitride quantum wells for all-optical switching via cross-phase modulation. © *2008 American Institute of Physics*. [DOI: 10.1063/1.2996107]

I. INTRODUCTION

Intersubband (ISB) transitions in GaN/Al(Ga)N quantum wells (QWs) have been the subject of extensive research efforts for the past several years.[1–17] These heterostructures are characterized by very large conduction-band offsets (up to about 1.75 eV) allowing for ISB transitions at record short wavelengths in the near-infrared spectral region. At the same time, they feature especially fast ISB relaxation lifetimes (a few hundred femtoseconds) due to the highly polar nature of (Al)(Ga)N. These properties are ideally well suited to the development of ultrafast all-optical modulators and switches operating at fiber-optic communication wavelengths. These devices in turn are expected to play a key role in next-generation optical communication networks to enable the implementation of basic signal processing functions directly in the optical domain at data rates of several hundred gigabit/s. Other wide-conduction-band-offset material systems currently being investigated for similar applications include InGaAs/AlAsSb (Ref. 18) and (CdS/ZnSe)/BeTe (Ref. 19) QWs.

In recent years, following extensive ISB absorption spectroscopy studies,[1–8] several basic device functionalities have been demonstrated with ISB transitions in GaN/Al(Ga)N QWs including photodetection,[9,10] electroabsorption modulation,[11,12] second harmonic generation,[13] and optically pumped light emission.[14] All-optical switching via ISB cross-absorption saturation in ridge-waveguide devices has also been demonstrated,[15,17] with the expected ultrafast recovery lifetimes. At the same time, control-pulse switching energies on the order of tens of picojoules have been reported, with a lowest value of 38 pJ for a 10 dB signal modulation depth obtained with an optimized waveguide structure.[17] These results strongly validate the promise of ISB cross-absorption saturation in nitride QWs for the development of ultrafast switching devices. An alternative approach to all-optical switching, with important potential advantages in terms of on-state losses, modulation depth, and noise-reduction regenerative capabilities,[20] is cross-phase modulation. In this case the control pulses are used to induce an ultrafast refractive-index change through a Kerr nonlinearity. The resulting phase modulation of the input signal is then converted into an amplitude modulation with an interferometric arrangement.

In general, ISB transitions can provide a large nonlinear refractive index with ultrafast response lifetime if the operating wavelength is properly detuned from the absorption peak.[21] In this paper we present an extensive investigation of this refractive-index nonlinearity in GaN/AlN QW waveguides designed for operation at fiber-optic communication wavelengths. In particular, in Sec. II we report the experimental demonstration of ISB self-phase modulation (SPM) in these devices, leading to a substantial spectral broadening of ultrafast near-infrared pulses. From the measured broadening, a nonlinear refractive index n_2 of 1.8×10^{-12} cm^2/W is estimated at the operating wavelength of 1550 nm. In Sec. III we then present a detailed theoretical model of the ISB refractive index of these devices as a function of wavelength and optical intensity. This model assumes an inhomogeneously broadened transition line and is almost entirely based on experimentally determined material and device parameters. Finally, in Sec. IV the results of this analysis are used to discuss the prospects of GaN/AlN QW waveguides for ultrafast all-optical switching via cross-phase modulation.

II. EXPERIMENTAL RESULTS

The QW material used in this work was grown by rf plasma-assisted molecular beam epitaxy on *c*-plane sapphire and consists of a 1.5-μm-thick AlN lower cladding layer, 30 repetitions of identical GaN/AlN QWs, and a 0.6-μm-thick

[a)]Electronic mail: rpaiella@bu.edu.

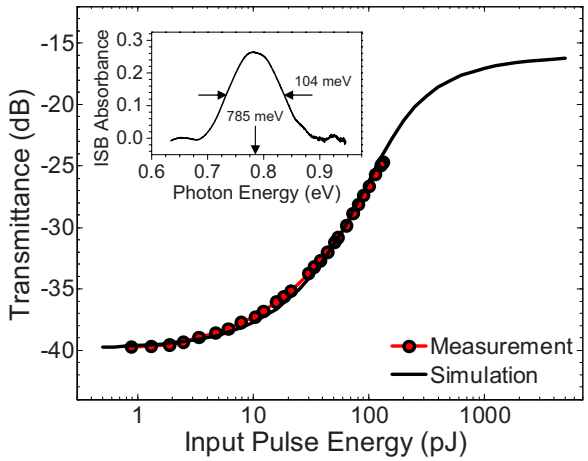

FIG. 1. (Color online) Circles: measured TM transmittance vs in-fiber input pulse energy for a GaN/AlN QW waveguide. Solid curve: numerical fit to the experimental transmittance data. Inset: measured ISB absorption spectrum of the waveguide QW active material.

GaN cap layer. The well and barrier layers have a thickness of 18 and 40 Å, respectively, selected so as to yield an energy separation between the lowest two conduction subbands in the 1.55 μm fiber-optic transmission window. A self-consistent Poisson–Schrödinger equation solver including the intrinsic electric fields of nitride heterostructures was used to design the QWs. The material ISB absorption spectrum was measured via Fourier transform infrared spectroscopy, using a sample that was mirror polished on the substrate side and lapped at 45° on two opposite facets to create a multipass wedge geometry. In particular, given the sample length of about 6 mm and thickness of 300 μm, the estimated number of passes through the active region is 20. As shown in the inset of Fig. 1, the measured absorbance spectrum is centered at a photon energy $h\nu_0$ of 785 meV (1.58 μm) and has full width at half maximum (FWHM) $h\sigma_{\mathrm{FWHM}}$ of 104 meV. Its peak value is 0.26, which corresponds to an ISB absorption coefficient of approximately 3.4×10^3 cm^{-1} as estimated using the procedure described in Ref. 22.

Ridge waveguides of different widths (etched through the entire thickness of the GaN cap) were fabricated with this material by photolithography and inductively coupled plasma reactive ion etching. In the resulting devices, the guided modes are confined in the higher-index GaN upper layer and overlap with the QW active region through their evanescent tail into the lower cladding. The thickness of the cap layer was selected to produce a fundamental guided mode with a narrow field profile peaked near the QWs, and correspondingly to maximize its overlap factor Γ with the QWs. At the same time, the fundamental mode has negligibly small amplitude near the sapphire/AlN interface, where a large density of material structural defects exists, which can cause large optical propagation losses. Bars containing several waveguides were then separated after scribing through the backside. Finally, the waveguide facets were carefully polished with fine diamond films to improve their optical quality, since a certain degree of roughness is sometimes created during bar separation due to the lack of common cleavage planes between *c*-plane sapphire and nitride epitaxial films. In the following, representative data measured with a 1-mm-long 3-μm-wide device are presented.

A detailed study of the transmission losses of these waveguides was carried out in Ref. 16 and is summarized in this paragraph as it provides some of the parameter values used in the theoretical model of Sec. III. The input and output coupling efficiency C and the nonsaturable propagation loss coefficient α_{WG} near 1.55 μm were measured via the cutback method, using waveguides with the same ridge structure just described but with thinner QWs providing negligible ISB absorption in this wavelength range. Values of $C=0.25$ per facet and $\alpha_{\mathrm{WG}}=2(4)\mathrm{dB/mm}$ for TE (TM) polarized light were determined with this procedure, using tapered fibers (polarization maintaining on the input side) to couple the light in and out of the waveguides. Incidentally, the measured 2 dB/mm excess TM losses may be attributed to charged edge dislocations parallel to the growth axis, which can effectively act as a wire-grid polarizer strongly suppressing TM light.[15]

Waveguides based on the aforementioned (18 Å)GaN/(40 Å)AlN QWs were then found to exhibit an additional saturable loss contribution in the 1.55 μm range for TM light only, which is ascribed to ISB absorption according to the polarization selection rules of ISB transitions in QWs. These saturable losses were studied using a passively mode-locked fiber laser with 20 MHz repetition rate, 1550 nm center wavelength, and 240 fs pulse width (as measured by autocorrelation after an identical fiber span). Exemplary data of overall TM transmittance versus in-fiber input pulse energy are shown in Fig. 1 (dotted curve). The fiber-to-fiber waveguide transmission losses at low input pulse energies in this case add up to about 40 dB. Accounting for the previously determined 4 dB/mm nonsaturable TM propagation losses and 12 dB (i.e., 0.25×0.25) total coupling losses, this corresponds to an unsaturated ISB absorption loss coefficient $\Gamma\alpha_{\mathrm{ISB}}^{\mathrm{unsat}}$ of 24 dB/mm. A large nonlinear saturation of the waveguide transmission losses is then clearly seen in Fig. 1 as the input pulse energy is increased, which can be exploited for all-optical switching via cross-absorption saturation. The solid line is a theoretical fit used to extract the ISB saturation intensity, as described in Sec. III.

Absorption saturation in these devices is accompanied by an ultrafast refractive-index modulation related to the same ISB carrier dynamics. Specifically, as electrons in the QWs are optically excited from the first to the second conduction subbands (at a rate proportional to the instantaneous intensity propagating in the waveguide), their contribution to the refractive index is temporarily bleached. As a result, a sufficiently intense pulse propagating through the waveguide can experience SPM, i.e., a time-dependent change in its optical phase directly proportional to its intensity waveform. This phenomenon in turn leads to the creation of new optical frequency components (i.e., spectral broadening), whose mutual interference typically leads to the appearance of characteristic oscillatory features in the pulse spectrum.[23]

This behavior has been clearly observed in the GaN/AlN QW waveguides studied in this work. To illustrate, in Fig. 2 we plot the optical spectra of TM- and TE-polarized pulses

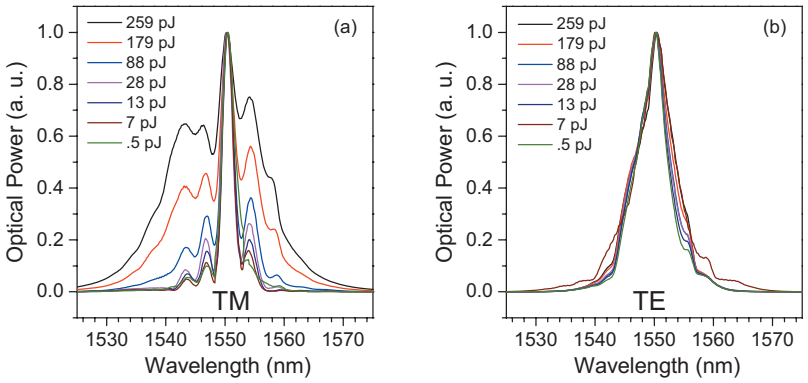

FIG. 2. (Color) Optical spectra of TM (a) and TE (b) pulses after transmission through a GaN/AlN QW waveguide for different values of the in-fiber input pulse energy.

measured after transmission through a 1-mm-long 3-μm-wide waveguide for different values of the in-fiber input pulse energy. All spectra have been normalized to unit peak value to more clearly display differences in their line shape. A particularly short (1 m) polarization-maintaining tapered fiber was used in these measurements between the mode-locked fiber laser and the waveguide in order to minimize the amount of temporal broadening and SPM experienced by the optical pulses in the fiber itself. The input pulse energy was varied by carefully moving the input tapered fiber away from the waveguide facet, so as to decrease the light intensity coupled into the device without changing the laser pumping conditions and hence the pulse intensity and waveform in the input fiber span. Similarly, the light polarization was changed by rotating the input fiber, i.e., without affecting the pulse path before the waveguide. The temporal width of the pulses launched onto the input facet is in this case 230 fs, again measured with a two-photon-absorption autocorrelation system after an identical fiber span.

As shown in Fig. 2(a), if the pulses are TM polarized so that they can couple to ISB transitions, they experience a large spectral broadening with increasing input power, which is attributed to the ISB refractive-index (and hence phase) modulation induced by the pulses themselves. In the low-power regime, the measured root-mean-square (rms) spectral width at the waveguide output is about 4 nm, roughly the same as that of the incident pulses. At pulse energies large enough to bleach the ISB transitions in the active layer, on the other hand, significantly broader output spectra are measured. At the same time, essentially no change in spectral shape with varying input power is observed with TE polarized light [Fig. 2(b)], which confirms the ISB origin of this nonlinear optical process. Regarding the detailed shapes of the TM spectra, they are presumably determined by the interplay between dispersion and nonlinear refraction in the waveguide, which is complicated by the strong wavelength dependence of the nonlinear index itself and by the fiber-induced chirp of the input pulses. Similarly, the shape differences between TE and TM spectra at low input powers are attributed to the different index dispersions experienced by the two polarizations in the device.

An estimate of the underlying nonlinear index n_2 can be obtained by noting that in the presence of SPM the rms spectral width is theoretically expected to double when[23,24]

$$\frac{2\pi}{\lambda}\Gamma n_2 \langle I_{\max}\rangle L = 1.97. \tag{1}$$

In this equation (which applies to the ideal case of unchirped Gaussian pulses in dispersionless nonlinear media), Γ is the overlap factor with the nonlinear medium, λ is the center wavelength of the pulse spectrum, and L is the waveguide length. Finally $\langle I_{\max}\rangle$ is the pulse peak intensity averaged over L, which can be related to the in-fiber input pulse energy approximately as follows:

$$\langle I_{\max}\rangle = \frac{1-e^{-\alpha_{\text{tot}}L}}{\alpha_{\text{tot}}L}\frac{CE_p}{A_{\text{eff}}\tau_p}, \tag{2}$$

where α_{tot} is the total propagation loss coefficient, C is the input coupling efficiency, A_{eff} is the modal effective area, and τ_p is the pulse width. In the present case we have $L=1$ mm, $\lambda=1550$ nm, $C=0.25$, and $\tau_p=230$ fs, as already discussed. A_{eff} and Γ are estimated to be 1.8 μm^2 and 5.3%, respectively, via a three-dimensional mode calculation based on the beam propagation method. The in-fiber input pulse energy E_p required to produce a factor-of-two rms spectral broadening is inferred from Fig. 3, where we plot the rms width of the measured TM spectra (normalized to its low-power value) versus in-fiber input pulse energy. A value of $E_p \approx 203$ pJ is estimated from these data. Finally, the value of α_{tot} corresponding to this input pulse energy is obtained from the transmittance data of Fig. 1 (subtracting the 12 dB coupling-loss contribution). The result is $\alpha_{\text{tot}} \approx 9$ dB/mm.

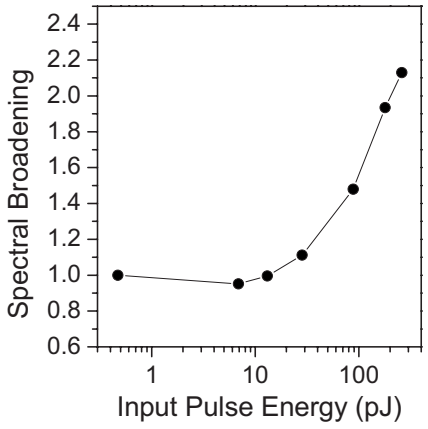

FIG. 3. Normalized rms width of the optical spectra of Fig. 2(a) vs in-fiber input pulse energy.

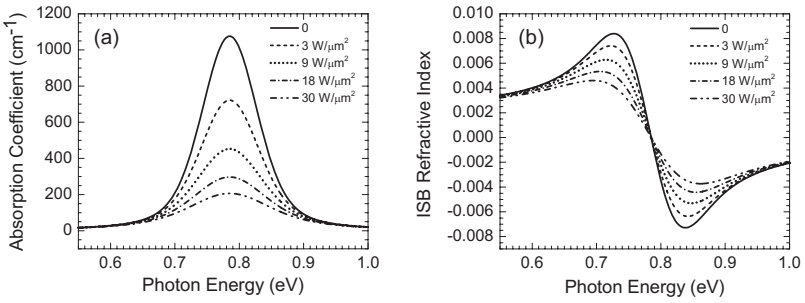

FIG. 4. Calculated ISB absorption coefficient (a) and ISB contribution to the refractive index (b) plotted vs photon energy for different values of optical intensity.

The nonlinear index n_2 of the QW active layer at 1550 nm is then obtained from Eqs. (1) and (2) using all the parameter values just described, giving an estimate of 1.8×10^{-12} cm^2/W. This value is in very good agreement with the results of a more detailed theoretical model described in the next section. At the same time, it is significantly larger than the value of 2×10^{-13} cm^2/W reported in the only previous direct measurement of n_2 in nitride QWs, where an unprocessed sample probed in a single-pass configuration was used.[3] Possible reasons for this large difference include a narrower ISB absorption linewidth in our sample, a better match between the excitation wavelength and that of maximum ISB nonlinear refraction, as well as the use of a waveguide geometry in our measurement.

III. THEORETICAL MODEL

To further investigate the ISB nonlinearities of these QW devices, we have developed a theoretical model where we first compute the ISB absorption spectrum as a function of optical intensity (based on the measurement results of the previous section), and then derive the associated refractive index via Kramers–Kronig transformations. Nitride QWs typically exhibit large ISB absorption linewidths mainly ascribed to thickness fluctuations.[1–6] Therefore, in this model we consider an inhomogeneously broadened ensemble of ISB transitions of center frequency ν_ξ governed by a Gaussian probability distribution of spectral width σ,

$$P(\nu_\xi) = \frac{1}{\sqrt{2\pi\sigma^2}} e^{-\frac{(\nu_\xi - \nu_0)^2}{2\sigma^2}}. \tag{3}$$

The overall ISB absorption coefficient is then written as[25]

$$\alpha_{\mathrm{ISB}}(\nu, I) = \alpha_0 \int_{-\infty}^{+\infty} d\nu_\xi P(\nu_\xi) \frac{L(\nu - \nu_\xi)}{1 + L(\nu - \nu_\xi)\frac{I}{I_{\mathrm{sat}}}}, \tag{4}$$

where

$$L(\nu - \nu_\xi) = \frac{(\Delta\nu/2)^2}{(\nu - \nu_\xi)^2 + (\Delta\nu/2)^2} \tag{5}$$

is the homogeneously broadened line shape function of the ISB transitions with center frequency ν_ξ.

In the present QW material, the average transition energy $h\nu_0$ is equal to 785 meV, as determined from the measured ISB absorption spectrum shown in the inset of Fig. 1. The FWHM $h\Delta\nu$ of the homogeneously broadened line shape function is taken to be 40 meV, based on a recent experimental report where such relatively large value was attributed to dephasing via electron-electron scattering.[6] The spectral width σ of the Gaussian distribution function describing the inhomogeneous broadening is then selected so that the overall FWHM of the absorption spectrum of Eq. (4) is equal to the measured value of 104 meV (again as determined from the inset of Fig. 1). The remaining two parameters required to evaluate Eq. (4) are the absorption strength α_0 and the saturation intensity I_{sat} of the homogeneous line. These are determined from the waveguide transmittance data of Fig. 1, in conjunction with the following differential equation describing propagation of TM light in the same waveguide,

$$\frac{dI}{dz} = -[\Gamma \alpha_{\mathrm{ISB}}(\nu, I) + \alpha_{\mathrm{WG}}]I. \tag{6}$$

This equation together with the initial condition $I(0) = (CE_p)/(\tau_p A_{\mathrm{eff}})$ can be used to calculate the waveguide transmittance $C^2 I(L)/I(0)$ at the experimental wavelength $\lambda = c/\nu$ of 1550 nm, as a function of in-fiber input pulse energy E_p. All required parameters are known (as discussed in the preceding paragraphs) except for α_0 and I_{sat}, which are then inferred by fitting the measured data of Fig. 1 to the calculated transmittance versus pulse energy. The best fit, given by the solid curve of Fig. 1, is obtained for $\alpha_0 = 2.2 \times 10^3$ cm^{-1} and $I_{\mathrm{sat}} = 3.9$ W/μm^2. Incidentally, this estimate for the ISB saturation intensity happens to be the same as the theoretical value reported in Ref. 26, which was computed using a self-consistent Poisson, Schrödinger, and rate equation solver.

In Fig. 4(a) we plot several calculated ISB absorption spectra for different values of the optical intensity inside the waveguide. The peak absorption coefficient in the fully unsaturated regime is 1.1×10^3 cm^{-1}, which is reasonably close to the estimate of 3.4×10^3 cm^{-1} obtained from the absorbance data of Fig. 1 (with the difference mainly attributed to epitaxial variations along the wafer area and to uncertainties in the above estimate). The expected saturation behavior is clearly shown in this figure. In particular, a factor of 2 decrease in peak value is obtained in the presence of about 6.4 W/μm^2 of propagating light, somewhat larger than I_{sat} because of the inhomogeneous nature of the transition broadening. It should be noted that the traces in this figure describe a situation where the absorption is both saturated and probed by the same wave at each photon energy (i.e., self-absorption saturation), which incidentally explains why no signs of spectral hole burning are observed. The associated contributions to the refractive index (n_{ISB}), computed via Kramers–Kronig transformations for each value of

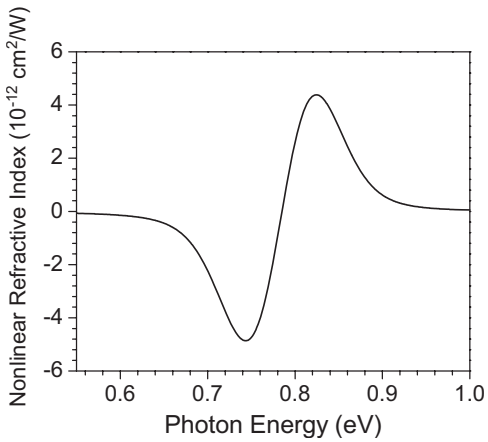

FIG. 5. Calculated nonlinear refractive index vs photon energy.

the optical intensity, are plotted in Fig. 4(b). As expected for a two-level system with a symmetric absorption line shape, both n_{ISB} and its intensity dependence exhibit a strong dispersion across the absorption bandwidth. In particular, the ISB refractive index is constant with intensity and equal to zero at the photon energy of peak absorption; vice versa, its absolute value and intensity dependence are largest near the half-width points in both directions.

Such large dispersion and complex intensity dependence imply that a description of ISB nonlinear refraction in terms of a constant nonlinear index n_2 is in general not appropriate. For the purpose of comparing this model with the results of Sec. II, we have however computed n_2 as a function of photon energy from the derivative $\partial n_{ISB}/\partial I$ in the limit of zero intensity [based on the Taylor-series expansion $n_{ISB}(I) = n_{ISB}(I=0) + n_2 I$]. The result is plotted in Fig. 5. At the photon energy of 800 meV used in our measurements (i.e., for $\lambda = 1550$ nm), this calculated nonlinear index is equal to 2.5×10^{-12} cm^2/W, in very good agreement with the value of 1.8×10^{-12} cm^2/W inferred from the data of Fig. 3 using Eq. (1). In any case, it is important to emphasize that both estimates involve a number of approximations, most notably in Eq. (1) the neglect of the nonlinear-medium dispersion and of the input pulse chirp, and in Fig. 5 the assumption of a linear relation between n_{ISB} and I. Thus, in general the full model for $n_{ISB}(\nu, I)$ described in this section–rather than the resulting estimate for n_2–should be used in the study of any nonlinear optical process related to ISB refractive-index saturation.

IV. CONCLUSIONS

The results plotted in Fig. 4(b) indicate that large refractive-index changes are induced in nitride QWs in the presence of optical pulses with peak intensities of a few tens of W/μm^2. Based on Eq. (2), under the experimental conditions used in this work such intensity levels can be produced throughout the waveguide with in-fiber input pulse energies of a few hundred picojoules (consistent with the data of Fig. 3). While such values are already experimentally accessible, a substantial reduction in the switching energy–by at least an order of magnitude–will likely be required before practical all-optical modulators and switches based on this nonlinearity can be developed. In this regard it is important to point out that several parameters of the present devices have large margins of improvement to further optimize the nonlinear response.

For instance, the input coupling efficiency C can be increased with the use of antireflection coatings and/or coupling optics providing a better match to the waveguide fundamental mode. Based on previously reported results with similar waveguides,[15,27] a factor of at least 2 improvement in C can be readily achieved, leading to a decrease in the required in-fiber control-pulse switching energy by the same amount. A similar improvement can be obtained using QWs providing ISB transitions at slightly longer wavelengths so that the effective nonlinear index is peaked at the desired operation wavelength of 1550 nm (cf. Fig. 5). The QW structural quality can also be further improved so as to decrease the absorption linewidth and correspondingly increase the ISB absorption and index nonlinearities. The present state of the art for near-infrared ISB transitions in GaN/AlN QWs is a Lorentzian (i.e., homogeneously broadened) absorption line with FWHM of 40 meV.[6] For such QWs, a maximum nonlinear index n_2 of 19.6×10^{-12} cm^2/W is computed using the model of the previous section, as opposed to 4.4×10^{-12} cm^2/W in Fig. 5. The QW doping level (which affects the absorption strength α_0) and the waveguide length L are two other adjustable parameters that can be used to optimize the tradeoff between transmission losses and nonlinear response. Finally, the homogeneous saturation intensity I_{sat} can also be decreased using more complex bandgap-engineered systems such as coupled QWs,[26,28] which incidentally have been recently demonstrated with nitride semiconductors.[7,8] For example, the simulations presented in Ref. 26 suggest that a 30 times decrease in I_{sat} can be obtained in these structures. With various combinations of these prescriptions, nitride QW waveguides are therefore promising for all-optical switching via cross-phase modulation with control-pulse energies of order 10 pJ and simultaneously ultrafast response times.

ACKNOWLEDGMENTS

This work was supported by NSF under Grant No. ECS-0622102.

[1] C. Gmachl, H. M. Ng, S.-N. G. Chu, and A. Y. Cho, Appl. Phys. Lett. **77**, 3722 (2000).
[2] N. Iizuka, K. Kaneko, and N. Suzuki, Appl. Phys. Lett. **81**, 1803 (2002).
[3] R. Rapaport, G. Chen, O. Mitrofanov, C. Gmachl, H. M. Ng, and S. N. G. Chu, Appl. Phys. Lett. **83**, 263 (2003).
[4] J. Hamazaki, S. Matsui, H. Kunugita, K. Ema, H. Kanazawa, T. Tachibana, A. Kikuchi, and K. Kishino, Appl. Phys. Lett. **84**, 1102 (2004).
[5] I. Friel, K. Driscoll, E. Kulenica, M. Dutta, R. Paiella, and T. D. Moustakas, J. Cryst. Growth **278**, 387 (2005).
[6] L. Nevou, M. Tchernycheva, L. Doyennette, F. H. Julien, E. Warde, R. Colombelli, F. Guillot, S. Leconte, E. Monroy, T. Remmele, and M. Albrecht, Superlattices Microstruct. **40**, 412 (2006).
[7] M. Tchernycheva, L. Nevou, L. Doyennette, F. H. Julien, F. Guillot, E. Monroy, T. Remmele, and M. Albrecht, Appl. Phys. Lett. **88**, 153113 (2006).
[8] K. Driscoll, A. Bhattacharyya, T. D. Moustakas, R. Paiella, L. Zhou, and D. J. Smith, Appl. Phys. Lett. **91**, 141104 (2007).
[9] D. Hofstetter, S.-S. Schad, H. Wu, W. J. Schaff, and L. F. Eastman, Appl. Phys. Lett. **83**, 572 (2003).
[10] A. Vardi, G. Bahir, F. Guillot, C. Bougerol, E. Monroy, S. E. Schacham,

M. Tchernycheva, and F. H. Julien, Appl. Phys. Lett. **92**, 011112 (2008).
[11]E. Baumann, F. R. Giorgetta, D. Hofstetter, S. Leconte, F. Guillot, E. Bellet-Amalric, and E. Monroy, Appl. Phys. Lett. **89**, 101121 (2006).
[12]L. Nevou, N. Kheirodin, M. Tchernycheva, L. Meignien, P. Crozat, A. Lupu, E. Warde, F. H. Julien, G. Pozzovivo, S. Golka, G. Strasser, F. Guillot, E. Monroy, T. Remmele, and M. Albrecht, Appl. Phys. Lett. **90**, 223511 (2007).
[13]L. Nevou, M. Tchernycheva, F. H. Julien, M. Raybaut, A. Godard, E. Rosencher, F. Guillot, and E. Monroy, Appl. Phys. Lett. **89**, 151101 (2006).
[14]L. Nevou, M. Tchernycheva, F. H. Julien, F. Guillot, and E. Monroy, Appl. Phys. Lett. **90**, 121106 (2007).
[15]N. Iizuka, K. Kaneko, and N. Suzuki, IEEE J. Quantum Electron. **42**, 765 (2006).
[16]Y. Li, A. Bhattacharyya, C. Thomidis, T. D. Moustakas, and R. Paiella, Opt. Express **15**, 5860 (2007).
[17]Y. Li, A. Bhattacharyya, C. Thomidis, T. D. Moustakas, and R. Paiella, Opt. Express **15**, 17922 (2007).
[18]A. V. Gopal, H. Yoshida, A. Neogi, N. Georgiev, T. Mozume, T. Simoyama, O. Wada, and H. Ishikawa, IEEE J. Quantum Electron. **38**, 1515 (2002).
[19]G. W. Cong, R. Akimoto, K. Akita, T. Hasama, and H. Ishikawa, Opt. Express **15**, 12123 (2007).
[20]B. Mikkelsen, S. L. Danielsen, C. Joergensen, R. J. S. Pedersen, H. N. Poulsen, and K. E. Stubkjaer, Electron. Lett. **32**, 566 (1996).
[21]M. Segev, I. Gravé, and A. Yariv, Appl. Phys. Lett. **61**, 2403 (1992).
[22]M. Helm, in *Intersubband Transitions in Quantum Wells: Physics and Device Applications I*, edited by H. C. Liu and F. Capasso (Academic, San Diego, 2000), Chap. 1.
[23]G. P. Agrawal, *Nonlinear Fiber Optics* (Academic, San Diego, 1995), Chap. 4.
[24]S. C. Pinault and M. J. Potasek, J. Opt. Soc. Am. B **2**, 1318 (1985).
[25]B. E. A. Saleh and M. C. Teich, *Fundamentals of Photonics* (Wiley, Hoboken, 2007), Chap. 14.
[26]Y. Li and R. Paiella, Semicond. Sci. Technol. **21**, 1105 (2006).
[27]R. Hui, Y. Wan, J. Li, S. X. Jin, J. Y. Lin, and H. X. Jiang, IEEE J. Quantum Electron. **41**, 100 (2005).
[28]G. Sun, J. B. Khurgin, and R. A. Soref, Appl. Phys. Lett. **87**, 201108 (2005).